Biogeochemistry (2005) 76: 113–139
DOI 10.1007/s10533-005-2671-3


# Understanding the anodic mechanism of a seafloor fuel cell: interactions between geochemistry and microbial activity

NATACHA RYCKELYNCK[1], HILMAR A. STECHER III[2] and CLARE E. REIMERS[2,*]

*[1]College of Oceanic and Atmospheric Sciences, Oregon State University, 104 Ocean Admin. Bldg., Corvallis, OR 97331-5503, USA; [2]College of Oceanic and Atmospheric Sciences, Oregon State University, Hatfield Marine Science Center, Newport, OR 97365, USA; *Author for correspondence (e-mail: creimers@coas.oregonstate.edu; phone: +541-867-0220; fax: +541-867-0221)*

Received 7 June 2004; accepted in revised form 18 February 2005

**Key words:** Anoxic sediments, Energy production, Fuel cell, Microbial activity, Pyrite, Sulfur

**Abstract.** Seafloor fuel cells made with graphite electrodes generate electricity by promoting electron transfer in response to a natural voltage difference (−0.7 to −0.8 V) between anoxic sediments and overlying oxic seawater. Geochemical impacts of a seafloor fuel cell on sediment solids and porewaters were examined to identify the anodic mechanisms and substrates available for current production. In an estuarine environment with little dissolved sulfide, solid-phase acid volatile sulfide and $Cr^{2+}$-reducible sulfur minerals decreased significantly toward the anode after 7 months of nearly continuous energy harvesting. Porewater iron and sulfate increased by millimolar amounts. Scanning electron microscope images showed a biofilm overcoating the anode, and electron microprobe analyses revealed accumulations of sulfur, iron, silicon and phosphorus at the electrode surface. Sulfur deposition was also observed on a laboratory fuel cell anode used to generate electricity with only dissolved sulfide as an electron donor. Moreover, current densities and voltages displayed by these purely chemical cells were similar to the values measured with field devices. These results indicate that electron transfer to seafloor fuel cells can readily result in the oxidation of dissolved and solid-phase forms of reduced sulfur producing mainly $S^0$ which deposits at the electrode surface. This oxidation product is consistent with the observed enrichment of bacteria most closely related to *Desulfobulbus*/*Desulfocapsa* genera within the anode biofilm, and its presence is proposed to promote a localized biogeochemical cycle whereby biofilm bacteria regenerate sulfate and sulfide. This electron-shuttling mechanism may co-occur while these or other bacteria use the anode directly as a terminal electron acceptor.

## Introduction

Organic carbon and S(-II) minerals constitute the most abundant reductants in recent marine sediments (Berner and Raiswell 1984). In highly productive areas (coastal zones and continental margins), organic carbon may accumulate at rates of 0.05–40 g C/m$^2$/y (Müller and Suess 1979; Walsh et al. 1985) creating sediments containing 0.5–20 dry-weight% $C_{org}$ (Jørgensen 1977; Müller and Suess 1979; Walsh et al. 1985; Canfield 1989b; Keil et al. 1994; Ransom et al. 1998). This organic matter fuels aerobic and anaerobic pathways of microbial respiration, depleting the sediment of dissolved oxygen while generating reduced

metabolites including $H_2S$ (Goldhaber and Kaplan 1975; Jørgensen 1977, 1982; Berner 1978; Canfield 1989b; Lin and Morse 1991). Dissolved sulfide may react with sedimentary iron to form a variety of iron-sulfide minerals, including amorphous-FeS, pyrrhotite $Fe_{(1-x)}S$ mackinawite $FeS_{(1-x)}$, greigite $Fe_3S_4$, and pyrite $FeS_2$ (with $x$ varying from 0 to 0.14; Berner 1970, 1984, 1985; Goldhaber and Kaplan 1975; Lin and Morse 1991; Wang and Morse 1996; Lin et al. 2002). Accumulation of sulfides with depth lowers sediment $C_{org}/S$ ratios to $\sim$3 on a weight basis (Berner and Raiswell 1984) and fixes the Eh of anoxic sediment at a potential on the order of 0.7–0.8 V lower than overlying oxic seawater (Baas Becking et al. 1960; Berner 1963; Jørgensen and Fenchel 1974).

Reimers et al. (2001) and Tender et al. (2002) investigated exploiting this potential difference for electrical energy using the principles of a fuel cell. Fuel cells, unlike batteries, are electrochemical devices continuously fed with electroactive compounds stored outside the cell (Bacon and Fry 1970; Greaves 1970; Vijh 1970; McDougall 1976). A seafloor fuel cell consists of an electrode buried in anoxic sediment (anode) and connected to another electrode positioned above in seawater (cathode). Dissolved oxygen present in bottom seawater is supplied as oxidant to the cathode, while the anode is in contact with local dissolved and solid-phase reductants. Reactions occurring at the anode surface have not yet been fully identified, but the oxidation rate of reduced species from the sediment appears to provide an upper limit to the overall rate of electrochemical reaction.

The present work highlights the use of sulfide minerals dispersed in sediments as electron donors to the fuel cell in a sulfide scavenging geochemical environment. This is in contrast to earlier experiments that indicated that current may be generated by dissolved sulfide oxidation (Tender et al. 2002) or direct electron shuttling by bacteria attached to electrode surfaces (Bond et al. 2002; Bond and Lovley 2003). By documenting fuel cell impacts on a variety of constituents present in porewater and solid phases, current production over a 7-month field demonstration is related to a unique anode-localized cycle of sulfur. Anode samples were also analyzed by scanning electron microscopy and electron microprobe to provide insight into electrode surface reactions that are coupled to transformations in an overlying biofilm and the adjacent sediment. To complete these investigations, a laboratory fuel cell was studied using only sterile solutions of dissolved sulfide as an electron source. The objectives of these tests were to quantify power densities obtainable by direct sulfide oxidation and to reveal newly formed oxidation products on anode surfaces.

## Experimental approach

### *Fuel cell deployment*

The prototype fuel cells deployed prior to the analyses in this study were fabricated from two 48.3 cm diameter $\times$ 1.3 cm thick graphite discs (extruded

graphite, grade G-10, Graphite Engineering and Sales, Greenville, MI) serving as electrodes and connected to a programmable resistive load (Model 870, Scribner Associates, Southern Pines, NC) as described in Tender et al. (2002). Each graphite disc was predrilled to have 790 evenly-spaced, 0.64 cm-diameter holes. Thus, the electrode geometric surface area was 0.542 $m^2$. Anodes and cathodes were fixed 30.5 cm apart within an open PVC frame that was partially buried by SCUBA divers. In this way, the electrodes were positioned parallel to and from 10–20 cm above and below the sediment–water interface, respectively. A control cell with unwired electrodes (open circuit) was deployed a few meters from the energy-harvesting 'active' device. The electronic device monitored the whole-cell potential (cathode vs. anode), half-cell potential (a bare Ag/AgCl reference electrode vs. anode) and current of only the active cell. These parameters were used to calculate the anode potential (anode vs. reference electrode), the cathode potential (cathode vs. reference electrode) and the electrical power (whole-cell potential × current). Current and power were normalized to the geometric surface area of the anode when computing current and power densities.

The location of the experiment was in Yaquina Bay, OR, at a water depth of 5 m at mean low water. Once in place, the active and control devices were influenced by a full range of environmental processes, including new sedimentation, sediment bioturbation, and tidal exchanges of bottom water. Two subminiature temperature recorders MDS Mark V/T (Alec Electronics Co., Kobe, Japan) were positioned next to the cathode and the anode of the active device and measured seawater and sediment temperature, respectively. The devices were monitored in place from June 28, 2001 to January 25, 2002.

## *Sample collection*

### *Sediment sampling*

Sediments surrounding both active and control devices were sampled with plastic core tubes (8 cm diameter by 30 cm long) at the end of the 7-month experiment. To remove sediment cores from above the active fuel cell anode, divers first removed the cathode from the PVC frame and brought it to the surface. Then they inserted three core tubes into the sediment down to the anode and capped them. The frame, anode, cores and sediment over the anode were then guided from the seafloor by the divers with the aid of a float bag. Once on the dock, these cores were lifted-off the anode with thin plastic plates that were inserted between the base of each tube and the anode. The cores were then transferred to a laboratory cold room (10 °C) for processing. In addition, after the cores were pulled, the entire anode (still covered with sediment) was removed to the laboratory cold room and placed in a glove bag under a positive pressure of flowing $N_2$ for further sampling.

Core sampling in proximity to the control cell was conducted differently. Two sediment cores were taken directly along side the control cell as close to the

anode as possible. These cores extended from the sediment–water interface down to about 5 cm below the anode. They were plugged at both top and bottom by the divers underwater and retrieved. The whole control device (with overlying sediment) was then removed and taken to the dock where it was disassembled. A third core (without any overlying water) was taken on the dock while the sediment column was still intact on the anode, and all the control cores were transported to the cold room. Lastly for additional sampling, the control anode with remaining sediment was also transferred to a glove bag that was keep under continuous $N_2$ flush to maintain an anoxic atmosphere.

*Anode sampling*

Sediments directly in contact with the active anode were observed to be lighter in color than overlying sediment layers. In order to document chemical reasons for this color change, two samples of the first 0.5 cm of sediment directly covering sections of the active anode were removed and set aside in centrifuge tubes while under a $N_2$ atmosphere. Pieces of exposed graphite surface from the active and control anodes were then gently rinsed of excess sediment using sterile artificial seawater, cut-off with a saw, rinsed again and immediately frozen in plastic bags flushed with $N_2$ for later surface analyses. Other areas of the anode surfaces were carefully washed with sterile artificial seawater and scraped with a sterile razor blade into 1.5 ml TE buffer (pH 8; Sigma, St. Louis, MO). These scrapings had the consistency of a cohesive biofilm. They were frozen for microbial 16S rDNA analyses described in Holmes et al. (2004b).

*Porewater extraction*

One core collected above the anode of both the active and control cells, and one core collected alongside the control was selected for sectioning and porewater extraction. Overlying water was treated the same as a sediment sample. Inside a glovebag thoroughly flushed with $N_2$, sediment was sliced into 0.5–2.0 cm sections, homogenized and transferred into acid-washed centrifuge tubes. The two extra samples collected directly from the active anode surface were processed as core slices. Sediment samples were centrifuged, and porewater was decanted and then filtered (0.45 $\mu$m) under a $N_2$ atmosphere in a clean glove bag. Centrifuge tubes containing the dewatered sediment were resealed while in the glove bag, and stored in $N_2$-filled bags at $-45$ °C for later analysis.

*Porewater analyses*

Aliquots of filtered porewater were immediately analyzed for total dissolved sulfide using a method modified from Cline (1969). Porewater subsamples were drawn under a $N_2$ atmosphere and then mixed with diamine reagent

concentration '*C*', diluted after full color development, and detected spectrophotometrically at 670 nm. Sulfate and chloride were determined after dilution of unacidified samples using a DX-500 ion chromatograph. Samples for iron and manganese (1.0–1.5 ml) were acidified with 10 $\mu$l 3.0 M HCl (TraceMetal Grade, Fisher Scientific) and analyzed after appropriate sample dilution by separate flow injection analysis methods (Resing and Mottl 1992; Measures et al. 1995). Silicate, phosphate and ammonium were determined using a nutrient autoanalyzer (Alpkem, Clackmas, OR) after appropriate dilution of unacidified samples. It was noted that some of the porewater samples appeared yellow and cloudy when exposed to air before nutrient subsamples were drawn. Later analyses revealed that these samples had high dissolved iron concentrations.

*Solid phase analyses*

A subset of sediment samples that had been processed for porewater chemistry was selected for solid phase analyses. Each analysis was run using triplicate subsamples. Each sample was homogenized before subsampling (in a glove box under $N_2$) and average wet/dry weight ratios were determined for each sample by weighing 0.5–1 g wet sediment in pre-weighed aluminum cups and drying these at 75 °C to a constant dry weight.

Iron oxides were extracted from other subsamples using freshly prepared oxygen-free reagents. Crystalline iron oxides (hematite, goethite, magnetite) were extracted in centrifuge tubes containing 0.5–1 g wet sediment with 20 ml dithionite solution (0.83 g sodium dithionite dissolved in 20 ml of 0.5 M sodium citrate/0.35 M acetic acid) by shaking for 4 h at 60 °C (Kostka and Luther 1994; Wijsman et al. 2001). Amorphous iron oxides ($Fe(OH)_3$, ferrihydrite) were extracted by shaking 0.5–1 g wet sediment in 20 ml ascorbate solution (ascorbic acid 22 g/l in 0.5 M sodium citrate/0.25 M sodium bicarbonate) for 24 h at room temperature (Ferdelman et al. 1991; Kostka and Luther 1994). After centrifugation, extracts were filtered through 0.45 $\mu$m Supor Acrodisc® syringe filters (Gelman) under a $N_2$ atmosphere and acidified with 100 $\mu$l 6 N HCl. Iron concentrations were measured in aliquots of the crystalline and amorphous Fe extracts diluted by factors of 1:100 and 1:10, respectively, using ferrozine and spectrophotometry (Stookey 1970). Volumes of 0.1 ml of reducing agent (15 g hydroxylamine hydrochloride dissolved in 150 ml 6 N HCl), 0.1 ml ferrozine (5.1 g/l) and then 0.1 ml buffer (60 g ammonium acetate dissolved in 52.5 ml ammonium hydroxide, diluted to 150 ml) were added successively to 5 ml of diluted samples. Each reagent addition was separated by 30 min to allow complete reaction, and samples were vortexed after each addition. Absorbances were read at 562 nm. Standards were prepared using electrolytic iron powder (<100 mesh, Fisher Scientific, Fair Lawn, NJ) dissolved in 0.6 N HCl and treated in the same way as extracted samples.

Reduced sulfur species were analyzed by a sequential extraction scheme. Acid volatile sulfides (AVS) were extracted from 0.2–0.5 g wet sediment for 2 h

by refluxing with 15 ml 1 N deoxygenated HCl under a continuous flow of $N_2$ (Zhabina and Volkov 1978; Allen and Parkes 1995). The liberated $H_2S$ was stripped from the solution with $N_2$ gas and trapped into a known volume (10–20 ml) of 1 M zinc acetate. A chromium reduction extraction was performed at the end of AVS extraction by adding 16 ml 1 N $CrCl_2$ in 0.5 N HCl and 8 ml concentrated HCl to the flasks (Canfield et al. 1986; Fossing and Jørgensen 1989; Wijsman et al. 2001). AVS traps were replaced with new traps containing 40 ml of 1 M $Zn(Ac)_2$ deaerated with $N_2$ between extractions. The acidified $CrCl_2$ solution was bubbled with $N_2$ at room temperature for 15 min followed by 45 min under a gentle reflux. This second extraction (henceforth referred to as determining chromium reduction sulfur or CRS) dissolves pyrite which is usually the most abundant sedimentary sulfur species in modern anoxic sediments but also includes the reduction of elemental sulfur to $H_2S$ (Zhabina and Volkov 1978; Allen and Parkes 1995). Sulfide concentrations were determined spectrophotometrically (Cline 1969). Standards were treated in the same way as ZnS precipitates.

Organic carbon and total nitrogen contents were determined with a CHN analyzer coupled with gas chromatography (Verardo et al. 1990) after exposure to acid fumes (concentrated HCl) for 24 h in order to eliminate inorganic carbon (mainly carbonate). Carbon and nitrogen were standardized with cystine, which contains 29.99 wt% C and 11.66 wt% N.

### *Sterile laboratory fuel cells*

To study the electroactivity of dissolved sulfide in the absence of other reductants or microorganisms, a 2-chamber fuel cell was constructed with 3-neck 500 ml aspirator bottles (Labglass, Buena, NJ), joined by two glass adapters inserted in the aspirator neck and connected by a pinch clamp (Ryckelynck 2004). Cathode and anode chambers were separated by a cation-selective membrane (Nafion117, Aldrich Chemical Company, Milwaukee, WI). Reagents, glassware and electrodes were autoclaved 20 min at 120 °C prior to two individual experiments (described below). Sterile 0.7 M NaCl was used as the electrolyte in both chambers, and the anode chamber was stirred continuously with a magnetic stirrer. The cathode chamber was open to the atmosphere and continuously aerated, while the anode chamber was purged with $N_2$ and then its headspace flushed with $N_2$ during and after sulfide additions. Air and nitrogen gas were passed through a 0.3 $\mu$m-pore size HEPA-VENT filter (Whatman). Electrodes were 46–49 mm long by 12.5 mm diameter graphite rods (extruded graphite, grade G-10, Graphite Engineering and Sales, Greenville, MI). Cathodes were soaked for 1 week in sterile 0.7 M NaCl to precondition the surface. The oxic chamber also contained a bare-wire Ag/AgCl reference electrode. Electrochemical data were recorded by a logging multimeter (Agilent 34970A; Agilent Technologies, Palo Alto, CA).

The two experiments were run for 6 days each. During both, the anoxic chamber was enriched with two 5 ml additions of 100 mM sterile $Na_2S$, one at the beginning and one after 3 days. In the first, whole-cell potential (cathode vs. anode) and anode potential (anode vs. reference electrode) were monitored at open circuit. In the second, a whole-cell potential of 0.3 V was imposed to discharge the cell after the first sulfide addition. This condition was controlled using a potentiostat Model DLK60 (Analytical Instrument System Inc, Flemington, NJ), while whole-cell potential, anode potential and current were recorded with the Agilent multimeter. Samples were regularly drawn from the anode chamber for dissolved sulfide analysis after Cline (1969). At the end of each experiment, pieces of graphite from the anode were cut and immediately embedded in epoxy (see below) for surface analysis.

### *Electron microprobe analyses and SEM images*

Anode surfaces from the Yaquina Bay and laboratory experiments were analyzed by electron microprobe and compared to unused graphite. Electrode pieces were mounted transversally and analyses were performed across and along the outer edge of the electrode. Graphite samples from the field experiment were first dried for 20 min at 40 °C and then mounted in standard epoxy resin (epo-kwick kit, Buehler LTD, Lake Bluff, IL). Samples from the laboratory experiments were directly embedded without drying in a hydrophilic epoxy (Nanoplast FB-101 embedding resin kits, SPI supplies, West Chester, PA) using a ratio of 30 g of melamine and 0.45 g of hardener. This epoxy was allowed to harden in an oven at 40 °C containing open containers of silica gel desiccant for 1 week. Sample polishing was carried out with progressively finer grades of abrasive, starting with sand paper and finishing with very fine alumina and diamond paste (METADI II Diamond Paste, Buehler LTD, Lake Bluff, IL). To avoid surface charging, each polished sample was carbon coated. Electron microprobe analyses were performed with an accelerating potential of 15.1 kV, a beam current of either 49.65 nA or 30.03 nA and a beam size of 5 $\mu$m. The electron microprobe was equipped with four wavelength-dispersive spectrometers. Scanning electron microscope (SEM) images were recorded in the backscattered electron mode to reveal differences in the composition (backscatter is a function of elemental mass) and to select areas for microprobe work.

## Results

### *The fuel cell*

Variations of whole-cell potential (WC), anode potential, cathode potential, current density, power density and temperature for the experiment in Yaquina

Bay are displayed in Figure 1. The system required 13 days after deployment to reach a near equilibrium potential (WC = 0.75 V). This state corresponded to cathode and anode potentials of 0.3 V and −0.45 V (vs. Ag/AgCl), respectively. Polarizations (Jones 1996) were applied on July 11th and 17th during which potential was lowered in steps of 0.01 V from 0.75 to 0.11 V. Each potential step was held for 3 min. The fuel cell responded instantly to each potential change, and for both polarizations the current density increased to a maximum of 110 $mA/m^2$ when the WC potential reached a minimum of 0.11 V. The WC potential recovered completely to an open circuit value of 0.76 V between the two polarizations.

During the next 4.5 months, the fuel cell WC potential was set at 0.27 V in order to draw near maximum power, and shifts in half-cell potentials and current were monitored. This part of the record is also reported in Tender et al. (2002) as daily averaged power densities (normalized to the anode footprint area). Cathode and anode potentials stabilized most often around 0.27 V (Figure 1c) and 0 V (Figure 1b) (vs. Ag/AgCl), respectively. Small variations in current tended to follow coupled half-cell potential oscillations, i.e., a voltage drop in both cathode and anode voltage coincided with a decrease in current. However, generally current increased during the first 6 weeks to reach a maximum value of 40 $mA/m^2$. The combination of constant WC potential and variable current resulted in an average power density of 11 $mW/m^2$ (Figure 1e).

An interruption in power generation occurred between September 22nd and October 3rd, 2001. During this period, the deployment site of the fuel cell was subject to high inputs of sedimentary material mixed with macroalgae that buried the cathode and eliminated the potential difference existing between cathode and anode environments, causing current flow to cease. Divers cleaned off the cathode and removed about 10 cm of new sediment from under the electrode. The system was then able to again draw current at a fixed cell potential of 0.27 V.

Current flow through the cell was turned off on November 30th due to an instrumentation problem with the Scribner 870, ending the part of the experiment when the WC potential was held at 0.27 V. With no current flow, the fuel cell voltage rose to 0.73 V (open circuit value) while the anode potential fell to −0.34 V. The Scribner 870 instrument was recovered from the seafloor leaving the electrodes in place and replaced by a new 870 programmable load located within the dockhouse above the experimental site. It was connected to the fuel cell through 30 m-long cables.

A constant current value of 10 mA (18 $mA/m^2$) was then imposed by the programmable load. During this period, the fuel cell maintained a WC potential of 0.30–0.35 V, with anode and cathode potential values of −0.05–0.00 V and 0.25–0.30 V, respectively. Shifts in WC potential were reflected primarily at the anode. The cathode potential was quite constant, showing only small regular oscillations, dominated by tidal cycles, also amplified by daily changes of temperature. Constant current and nearly steady cell voltage

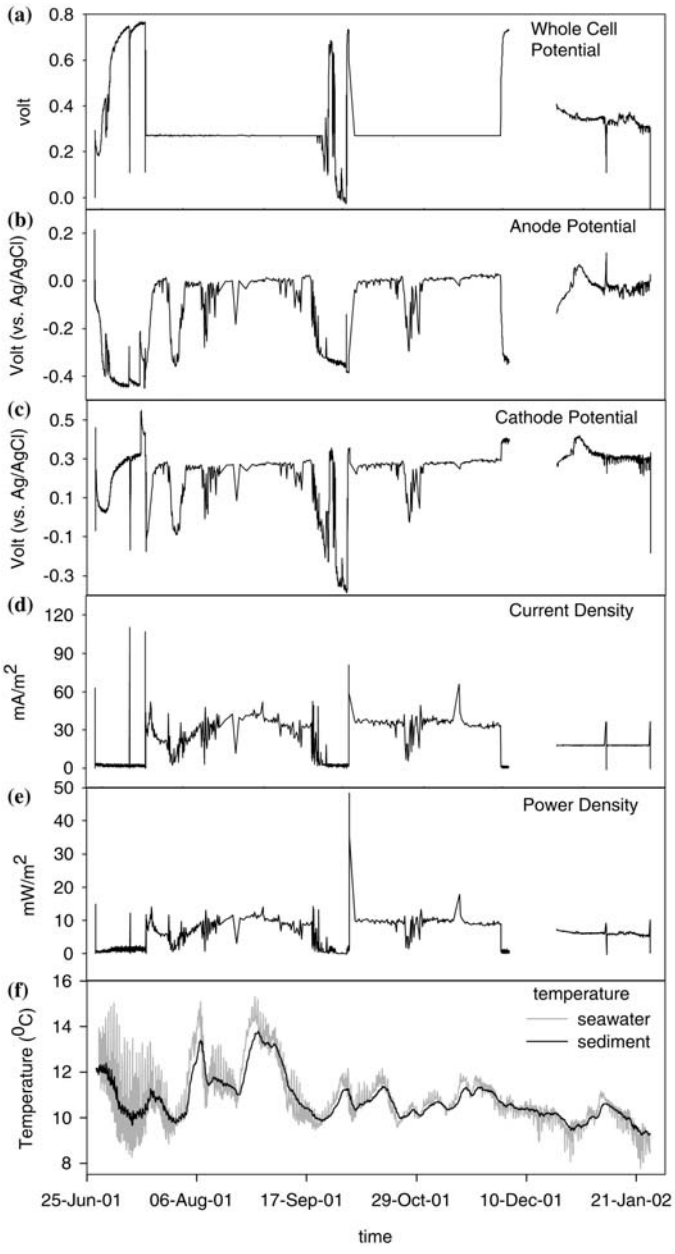


*Figure 1*. Whole-cell potential (cathode–anode) (a), anode potential (anode–reference) (b), cathode potential (cathode–reference) (c), current density (d) power density (WC potential × current density) (e) and temperature (f) recorded during the 7-month experiment in the Yaquina Bay Estuary. The cathode half-cell potential and the power density were calculated from the measured parameters (WC potential, anode potential and current). Current and power values were normalized to the total anode surface area (0.542 $m^2$).

produced a power density of about 6 $mW/m^2$. The system was able to sustain 10 mA (18 $mA/m^2$), indicating the sources of reductants in the sediment were sufficient to continuously provide electrons to the anode. In contrast, when the current density was temporarily raised to 36 $mA/m^2$ on January 9, the WC potential collapsed to 0.10 V over 6 h lowering the power density to 3.6 $mW/m^2$ (Figure 1d and e).

*Sediment geochemistry*

Profiles of porewater and solid-phase compounds from the Yaquina Bay sediment cores (Figures 2 and 3) display typical overall patterns for a subtidal estuarine environment (Powell 1980). These profiles are referred both to the position of the active anode (left *Y* axes of Figures 2 and 3) and the seafloor/seawater interface (right *Y* axes of Figures 2 and 3).

At both active and control sites dissolved oxygen was depleted in the first few millimeters of the sediment column (data not shown). Dissolved iron and manganese distributions were characterized by subsurface peaks with respective peak concentrations of 96 and 8 $\mu$M, three centimeters below seawater-sediment interface (Figure 2c and d) indicating the presence of a suboxic zone where organic matter oxidation is associated with the microbial reduction of Fe and Mn oxides. Sulfate concentrations were nearly constant at approximately 21 mM in the Fe/Mn reduction zone and then decreased to 14 mM at the active site (Figure 2b). Profiles of sulfate/chloride ratio (data not shown) have patterns similar to sulfate alone due to relatively small downcore variations of chloride concentration ($<10\%$) (Figure 2e). This indicates sulfate variations cannot be attributed to dilution effects associated with inputs of lower salinity estuarine waters. Instead, sulfate depletion is a consequence of microbial sulfate reduction (Jørgensen 1977). The lack of a sulfate gradient and the smaller increases in ammonia (Figure 2f) and phosphate (Figure 2g) between $-10$ and $-20$ cm depth at the control compared to the active site suggest that sulfate reduction rates were lower in sediments surrounding the control device.

A second form of evidence for relatively higher sulfate reduction rates at the active site is that the organic matter content was greater near the sediment–water interface than at the control site (Figure 3a and b). Furthermore, Figure 2a shows sulfide maxima (50–150 $\mu$M) 8–10 cm below the seafloor boundary with higher concentrations over the active anode. The near absence of sulfide within deeper parts of the profiles also corresponds to a significant loss of amorphous Fe (20–70 $\mu$mol Fe/g dry sediment) (Figure 3d) and crystalline Fe (50–100 $\mu$mol Fe/g dry sediment) (Figure 3c). Indeed in coastal sediment, Fe(III) acts as a sink for dissolved sulfide, leading to the formation of iron sulfide minerals (Canfield 1989a; Thamdrup et al. 1994; Thamdrup and Canfield 1996). This is consistent with the increase of FeS that can be detected as AVS, which was highest over the active anode (80 $\mu$mol S/g dry sediment) at a depth of $-10$ cm (Figure 3e) corresponding to the depth where the dissolved

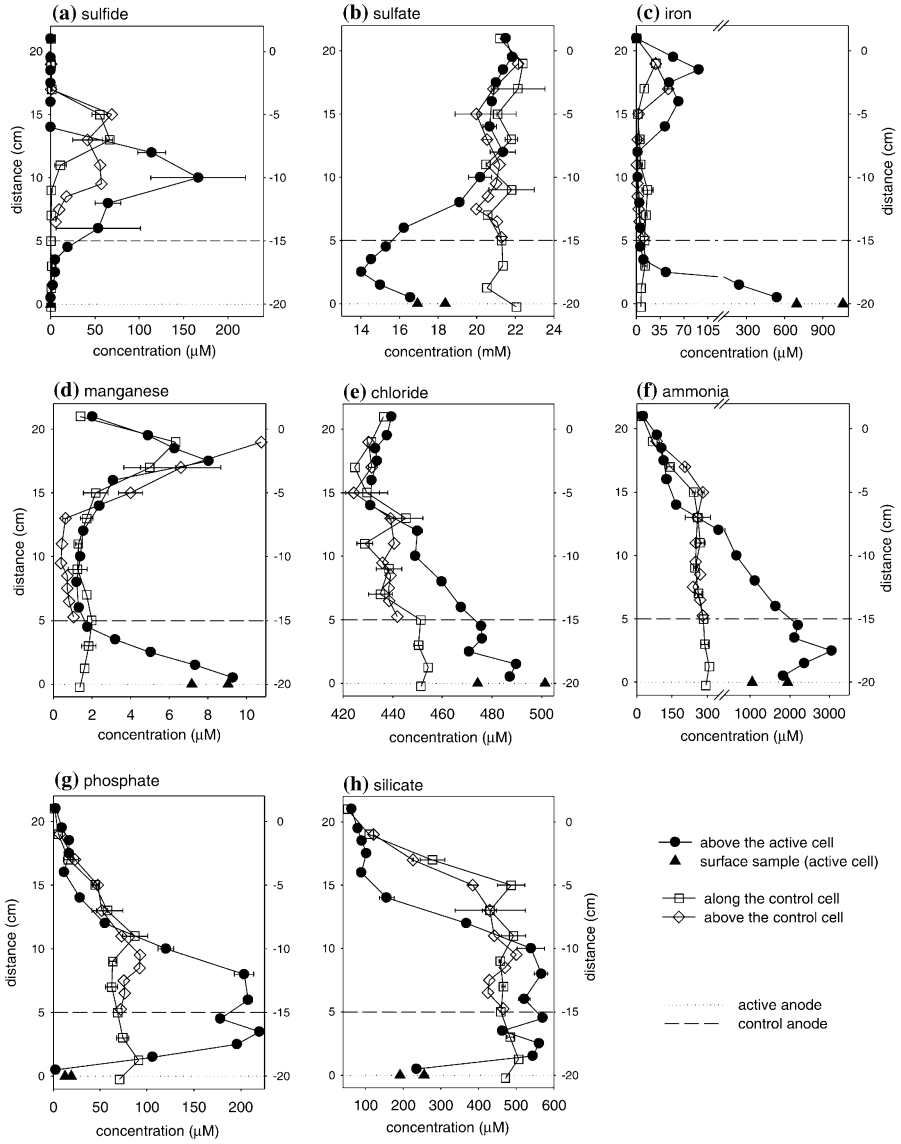


*Figure 2*. Porewater profiles associated with the experiment in Yaquina Bay Estuary. Distributions of dissolved species from along side and above the control graphite electrode and above the anode of the energy-harvesting fuel cell are presented. The active anode was located at a sediment depth of 20 cm at the time of recovery (dotted line level), while the control anode was positioned 5 cm shallower (dashed line level). Error bars correspond to plus or minus one standard deviation of duplicate sediment samples processed from the same depth interval.

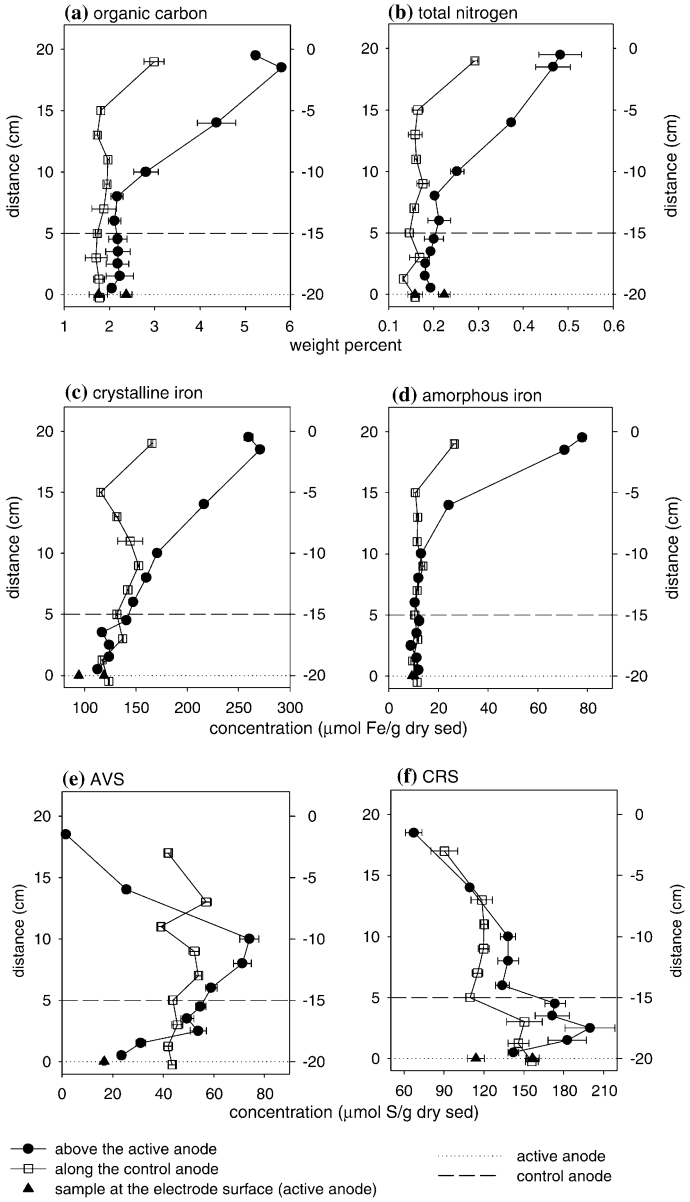


*Figure 3.* Solid phase profiles associated with the experiment in Yaquina Bay Estuary. Notations are the sample as in Figure 2. Error bars correspond to plus or minus one standard deviation of samples analyzed in triplicate.

sulfide concentration was maximal. Beneath this peak, the AVS content decreased gradually to 20 $\mu$mol S/g dry sediment. This trend is consistent with the transformation of metastable iron sulfide compounds to $FeS_2$ (Berner 1964)

but was not as pronounced at the control site. CRS increased generally with depth from 60 $\mu$mol S/g dry sediment to 150–200 $\mu$mol S/g dry sediment (Figure 3f).

Sediments in close contact with graphite electrodes showed significant profile shifts at the active site only. Figure 2b–d indicate large enrichments of dissolved iron (up to 1 mM), sulfate (3–5 mM) and manganese (6–8 $\mu$M) in porewaters within a 3 cm-thick zone approaching the active anode but not near the control anode. Phosphate, silicate and ammonia profiles display abrupt reversals over the same intervals (Figure 2f–h). Organic carbon and total nitrogen distributions were similar immediately above the control and active anodes, with respective concentrations of 1.8–2.3% and 0.15–0.22% below 12 cm from the sediment/seawater interface Figure 3a and b). Amorphous and crystalline iron oxides also did not appear affected by the presence of the fuel cell (Figure 3c and d). CRS and AVS decreased by 100 $\mu$mol S/g dry sediment and by 40 $\mu$mol S/g dry sediment, respectively, toward the anode of the active cell, whereas profiles from the control site indicated no losses of reduced sedimentary sulfur (Figure 3e and f).

### *Anode surfaces*

Microorganisms in the *Desulfobulbus*/*Desulfocapsa* cluster were the predominant bacteria attached to the active anode and accounted for 100% of the $\delta$-Proteobacterial sequences identified from 16S rDNA clone libraries constructed from extracted DNA (Table 1). In contrast, *Desulfobulbus*/*Desulfocapsa* spp. were relatively less enriched on the control electrode. These sulfate-reducing bacteria are known for their capability of deriving energy for growth from the disproportionation of $S^0$ when sulfide concentrations are low (Lovley and Phillips 1994; Finster et al. 1998). The control anode also differed from the active electrode in yielding a high diversity of microbial DNA including other sulfate-reducing bacteria in the $\delta$-Proteobacteria group. A detailed report of these results and comparison to microbial communities

*Table 1.* Relative proportions of the major phylogenetic groups of bacteria identified from 16S rDNA sequences recovered from the anodes of the active and the control cells deployed in the Yaquina Bay Estuary, from Holmes et al. (2004b).

| Bacterial group | Related genera | Estuary | |
|---|---|---|---|
| | | Active fuel cell | Control cell |
| $\alpha$-Proteobacteria | | – | 7.1% |
| $\delta$-Proteobacteria | *Desulfobulbus* spp./*Desulfocapsa* spp. | 62.5% | 11.9% |
| | *Sulfate reducing* | – | 23.8% |
| $\gamma$-Proteobacteria | | – | 16.7% |
| Cytophagales | | 32.5% | 9.5% |
| Other bacteria | | 5% | 28.6% |

associated with electrodes from other aquatic sediments can be found in Holmes et al. (2004b).

Backscattered electron (BSE) images of sections of the Yaquina Bay electrodes revealed some similar compositional features at both control and active anode surfaces (Figure 4). Both graphite sections were covered with a 200–250 $\mu$m thick layer, indicating the presence of a biofilm. The main difference between the active and control cell samples occurred at the graphite/biofilm interface: a separate layer between the two phases was clearly apparent in images of the active anode, but hardly visible in images of the control anode (Figure 4).

The elemental composition of the biofilm and the interface layer was quantified by electron microprobe. Figure 5a shows elemental profiles across the anode surface of the active fuel cell. Nitrogen was quite homogeneously distributed in the biofilm, showing concentrations between 2 and 5 wt% (Figure 5a), except in areas of very high Si concentration (Figure 5a). This pattern was a consequence of the presence of mineral grains corresponding to the bright spots on the BSE images (Figure 4). However, all Si profiles showed a similar peak reaching 10 wt% 10–20 $\mu$m above the graphite interface (Figure 5a). This zone also exhibited elevated iron and sulfur concentrations. These elements respectively reached 1.0–1.3 wt% and 1.6–2.0 wt% (Figure 5a). The biofilm also stored a significant amount of sulfur (between 1.0 and 1.5 wt%) but was not enriched in iron (less than 0.1%). Phosphorus profiles showed a distribution pattern similar to Fe, with low content (0.02–0.04 wt%) in the biofilm and an increase of concentration to 0.16 wt% at the graphite surface (Figure 5a), where iron deposition was greater.

Elemental distributions were also measured along the surfaces of the anode samples. Figure 5b indicates deposition of sulfur and iron on the active anode but not on the control anode. The control electrode exhibited contents of these elements similar to the reference sample of unused graphite. Iron and sulfur were respectively 400 times and 20 times more abundant at the electrode surface of the active fuel cell. Fe/S atomic ratios were generally less than 1.

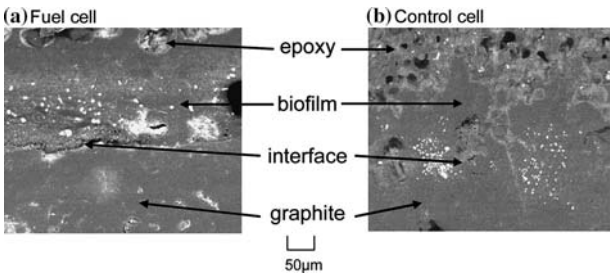


*Figure 4*. Backscatter electron microscope images of surface cross-sections of the graphite electrodes that were buried in Yaquina Bay.

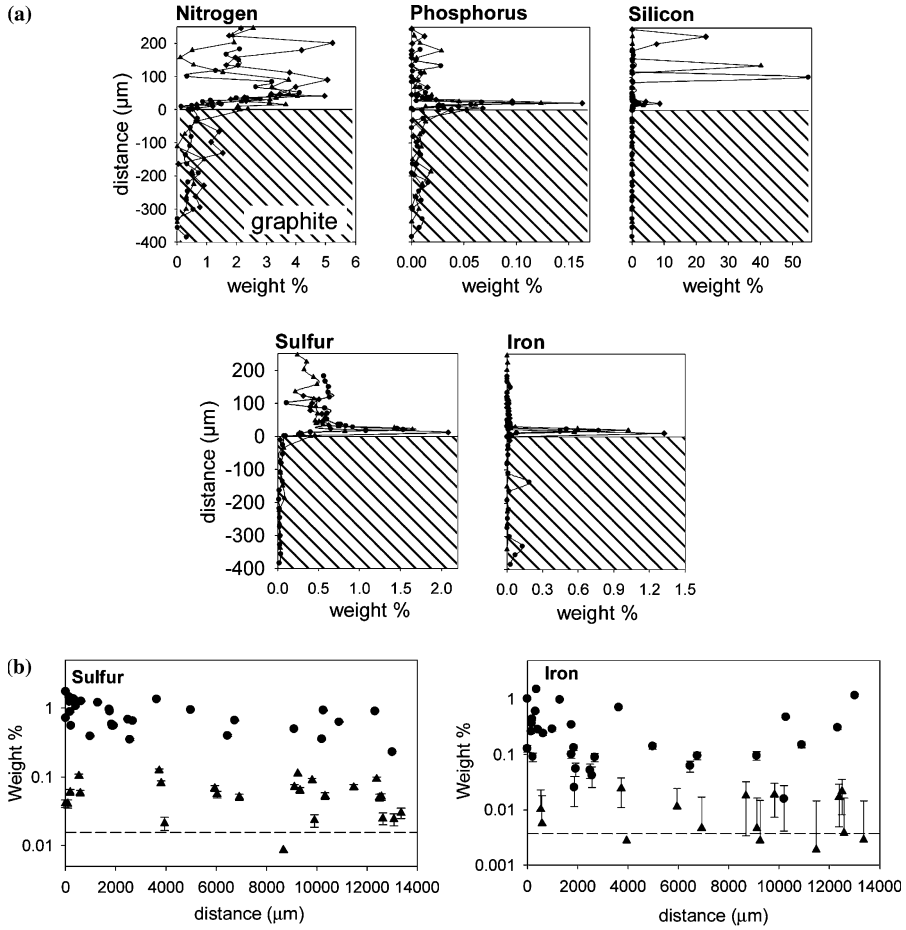


*Figure 5.* (a) Electron microprobe profiles across the interface of the energy-harvesting graphite anode deployed in the Yaquina Bay Estuary. The electrode surface is at 0 $\mu$m; patterned area (with negative distance) represents the graphite material; positive distance numbers are located in the biofilm. (b) Sulfur and iron concentrations along the interface of the active and control graphite anodes compared to a reference sample mean (unused graphite) (note log scale).

## *Laboratory simulations*

The two laboratory simulations were run to verify the role of sulfide as an electron donor and to determine its short-term effect on anode surfaces. Figure 6a shows the anode potentials for both open circuit and discharge experiments, and Figure 6b illustrates the current density measured during the discharge. The potentials decreased rapidly when sulfide was added at the beginning of both experiments. The anode voltage of the open circuit experiment never fully stabilized: it slowly decreased to attain −0.52 V (vs. Ag/AgCl)

after 6 days. The corresponding WC potential was 0.75 V. This is close to the open circuit value observed in the estuarine environment (Figure 1). In contrast, in response to the imposed whole-cell value of 0.3 V, the anode potential during the second experiment was relatively steady at a value of −0.22 to −0.25 V (vs. Ag/AgCl). The second addition of sulfide after 72 h caused the anode potentials to shift by −0.02 V in both experiments (Figure 6a). Before this injection of sulfide, the open circuit and discharging chambers contained 0.83 and 0.79 mM, respectively, and the second sulfide addition raised these concentrations to 1.52 and 1.56 mM. The small difference in concentration between both experiments was a consequence of the subsampling that altered the quantity of medium present in the chambers. The curve describing the current production (Figure 6a) started (once the potential difference was imposed) with a spike of current (32 $mA/m^2$) that decreased rapidly at first. The second sulfide addition did not generate another spike of current, only an increase from 8 to 15.5 $mA/m^2$. The system also exhibited small diurnal variations with steady currents during the day and small decreases at night. At the end of the control and energy-harvesting experiments, sulfide concentrations were 1.36 and 1.33 mM, respectively, representing sulfide losses of 10.5 and 14.5%.

Quantitative electron microprobe data was used to compare the graphite surface to the underlying graphite (similar transects 50 $\mu$m below the surface) of the two anodes. The surface of the discharged fuel cell anode presented a relative enrichment of sulfur between 24 and 70%, while the surface of the open circuit anode had on average 18% more S (Figure 6b). Some of this S may have been derived from seasalt taken up by the Nanoplast FB-101 resin that was observed in elemental maps to have a background S content not seen in the standard epoxy used when embedding the pre-dried field electrode samples (see Methods). Transects along the surface of the current-passing anode also indicated that S was distributed unevenly.

## Discussion

### *Direct and indirect sources of electrons*

The two-chambered laboratory experiments confirmed dissolved sulfide can serve as a direct source of electricity when simulating a seafloor fuel cell. Although biogeochemically much simpler than marine sediments, the two-chamber electrochemical cells reached WC and anode potentials at open circuit (Figure 6a) similar to those observed during the Yaquina Bay experiment (Figure 1a and b). This supports previous laboratory and field studies (Berner 1963; Jørgensen and Fenchel 1974) that have concluded that the reversible half-cell between sulfur and sulfide often regulates the potential difference between seawater and anoxic sediment. Earlier electrochemical studies by Allen and Hickling (1957) also attribute anode voltages from approximately −0.47 to

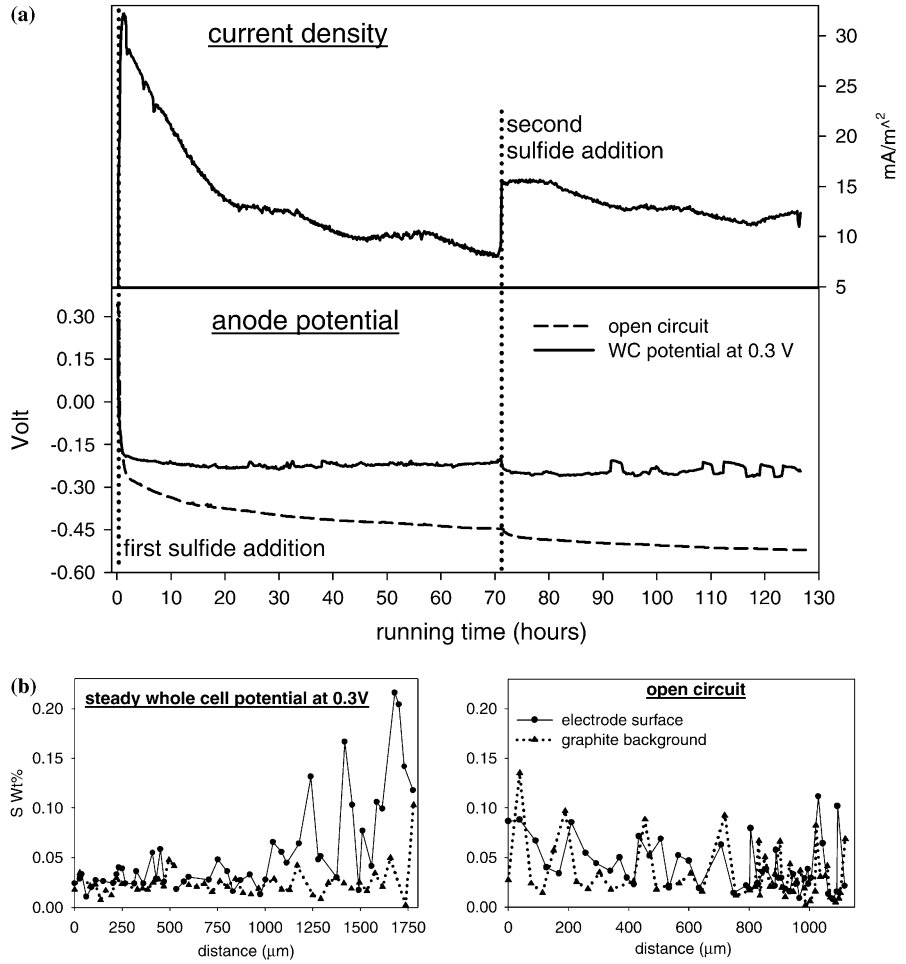


*Figure 6*. (a) Variations in the anode potential (vs. Ag/AgCl) and current density during the laboratory simulations run for 6 days. The control experiment was run at open circuit. (b) Comparison of sulfur deposition between the open circuit and the energy harvesting laboratory experiments; measurements by electron microprobe of sulfur content at the electrode surface and in the underlying graphite material for both experiments.

−0.57 V (vs. a saturated calomel reference) to the equilibrium potential of a sulfur–sulfide system at varying concentrations of dissolved sulfur and sodium sulfide under alkaline conditions.

Sulfide losses during the discharge experiment may be compared to the electrochemical oxidation rate indicated by the current record. Current was integrated over time and converted to moles of electrons. In total 130 $\mu$moles of electrons were exchanged during the experiment. Assuming the oxidation of sulfide was to elemental sulfur (Ateya and Alkharafi 2002a, b; Ateya et al.

2003), 65 $\mu$moles of sulfide must have been oxidized. This represents only 4% of the total amount of sulfide present in the system suggesting that the total exchange of electrons was limited by electrode area and electrode kinetics (Ateya and Alkharafi 2002b). Total sulfide losses (14.5%) are believed to have resulted from $H_2S$ degassing or oxidation during the sampling of the anode chamber in addition to electrochemical oxidation at the anode. Indeed, as described in the methods section, the anode chamber was opened frequently in order to pipette out enough solution for sulfide analysis. This sulfide balance is also consistent with the sulfide losses observed during the open circuit experiment (10.5%).

The current increased when sulfide was added to the system (Figure 6a). This indicates that the oxidation of dissolved sulfide is controlled by charge transfer at the electrode/electrolyte interface and by diffusion from within the electrolyte across the electrode double layer (Ateya and Alkharafi 2002b). The early exponential decay of current with time can be attributed to passivation of the electrode surface (Ateya et al. 2003), rather than a reduction in the sulfide flux due to consumption. The diurnal oscillations exhibited in current density (Figure 6a) were probably a consequence of changes in light or/and temperature in the laboratory. Such variations were also observed during the Yaquina Bay experiment. Ateya et al. (2003) demonstrated that temperature influences the rate of sulfide oxidation: lower temperature (e.g., at night) resulted in a decrease in current. Thus physical parameters influence the kinetics of electrochemical reactions, and these effects are reflected in the number of electrons exchanged.

During the experiment in Yaquina Bay, it is likely that any supply of dissolved sulfide to the anode was severely limited by the low porewater concentrations at the anode depth (modulated by the activity of sulfate-reducing bacteria and reactions with iron) and diffusion in porewater. Porewater distributions like those displayed in Figure 2 can be found year-round with the exception that the near surface peaks in Fe and sulfide are often greater during late summer months (Reimers unpublished data). Therefore other sources of reductant must have interacted to continuously sustain the current production (Figure 1d). Figure 3e and f show that reduced sulfur minerals were lost from the sediments under the effects of the fuel cell. The dissolution of these compounds by anodic oxidation may have provided electrons to the electrode sustaining the production of electricity. Possible half-cell reactions suggested from electrochemical studies (Hamilton and Woods 1981; Turcotte et al. 1993; Holmes and Crundwell 2000) are the oxidation of any of the metastable iron sulfides (which for simplicity we will assume have an Fe:S stoichiometry = 1)

$$FeS \rightarrow Fe^{2+} + S^0 + 2e^- \quad (1)$$

the direct oxidation of pyrite to sulfur

$$FeS_2 \rightarrow Fe^{2+} + 2S^0 + 2e^- \quad (2)$$

or pyrite oxidation to sulfate

$$FeS_2 + 8H_2O \rightarrow Fe^{2+} + 2SO_4^{2-} + 16H^+ + 14e^- \quad (3)$$

Ferrous iron is not oxidized according to these reactions but is released to solution.[1] In nature, the most important oxidants that can react with sulfide minerals are $O_2$ and $Fe^{3+}$ (Moses et al. 1987; Moses and Herman 1990; Schippers and Jørgensen 2002; Rimstidt and Vaughan 2003). For electrochemical oxidation to occur at a graphite electrode, neither of these oxidants need interact directly with mineral surfaces. Instead, the anode must be at a raised potential for electron transfer to occur from the mineral to the anode. At this time, it is unknown if electron-shuttling mediators or microorganisms play a role or whether mineral grains must contact the anode surface. One hypothesis, related to the semi-conductor properties of iron sulfides (Mycroft et al. 1990; Holmes and Crundwell 2000), suggests that electrons could be shuttled along mineral grains to the electrodes. Mycroft et al. (1990) have detected the formation of polysulfides at the surface of pyrite particles under conditions of anodic oxidation and attributed these products to this process. Additionally, localized bioturbation may act to randomly move sulfide minerals to the region of anode influence, thereby gradually creating a concentration gradient away from the anode.

### *Oxidation products: elemental sulfur, sulfate and iron*

The surface analysis of the anodes of the laboratory and field fuel cells revealed sulfur enrichments at the electrode surface (Figures 5 and 6b). Ateya et al. (2003) used X-ray Photoelectron Spectroscopy to identify $S^0$ as the product of the electrochemical oxidation of sulfide on graphite electrodes. This is in agreement with a mechanism proposed by Allen and Hickling (1957) who suggested that the initial step of sulfide oxidation on an inert electrode is the adsorption of a polysulfide ion $S_x^{2-}$, followed by reaction with a further polysulfide ion to produce $S^0{}_{x-1} + S_{x+1}{}^{2-}$. Further, Hamilton and Woods (1981) observed $S^0$ as the dominant surface product of FeS and pyrite oxidation; however, the proportion of sulfate produced increases as the anode potential is taken to higher values and at higher pH.

Turcotte et al. (1993) and Zhu et al. (1994) argued that electrodeposited elemental sulfur is a form of sulfur that has much better conducting properties

[1]As will be noted in the following section, we do not fully rule out iron oxidation as an anode reaction. Iron oxidation would have been possible at some of the highest anode potentials measured infrequently during the Yaquina Bay experiment according to the electrochemical studies of Hamilton and Woods (1981). We have run experiments similar to the laboratory simulations described in this paper, but with 1 mM $Fe^{2+}$ added as $Fe(NH_4)_2(SO_4)_2{\cdot}6H_2O$ to sterile, deoxygenated seawater and generated short-term (but not sustainable) current densities of $\sim$7 $mAm^{-2}$ at 0.3V. However, the accumulation of porewater Fe in the vicinity of the active field-deployed anode suggests Fe oxidation was not a major electrode reaction over the many months in the field.

than bulk $S^0$ in its orthorhombic state. This implies that such $S^0$ can be further oxidized or reduced, depending on the potential conditions. Elemental sulfur oxidation (or reduction) may also be microbially mediated. For example, species of the *Desulfobulbus*/*Desulfocapsa* genera have been shown to disproportionate elemental sulfur when sulfide levels are low (Lovley and Phillips 1994; Finster et al. 1998).

$$4S^0 + 4H_2O \rightarrow SO_4^{2-} + 3HS^- + 5H^+ \quad (4)$$

Holmes et al. (2004a) also demonstrated the ability of *Desulfobulbus propionicus* bacteria to oxidize $S^0$ to $SO_4^{2-}$ with an electrode serving as an electron acceptor. Either of these oxidation pathways from elemental sulfur to sulfate is consistent with the increase in $SO_4^{2-}$ detected above the active anode (Figure 2b).

The enrichment in dissolved iron (and to a much lesser extent manganese) approaching the anode may be explained by the liberation of these metal ions during the anodic oxidation of sulfide minerals. In addition, some $Fe^{2+}$ may be oxidized at the anode surface depositing $Fe^{3+}$ species that may adsorb or co-precipitate with phosphate and silicate (Rozan et al. 2002; Pokrovski et al. 2003). Dissolved species of P, N and Si were all seen to exhibit porewater gradients approaching the anode and to be enriched at the anode surface (Figure 5). We can not provide reaction-specific explanations for these results without further experimentation. However, in independent laboratory studies utilizing microelectrodes, we have shown decreases in pH of approximately 0.6 units approaching anodes drawing current from Yaquina Bay sediments (Reimers, unpublished data). This pH shift is consistent with reaction (3) or the oxidation of dissolved $HS^-$. It would also influence specific precipitation and adsorption reactions such as the binding of phosphate and silicate to a graphite surface or to iron oxyhydroxides (Stumm 1992).

### *Electron balance between produced current and geochemical reactions*

The importance of electrochemical reactions involving sulfur minerals for sustaining current over the operating life of a seafloor fuel cell may be evaluated by comparing mineral losses to the total electron budget. In the case of the Yaquina Bay experiment, the total current produced over 7 months was estimated by integrating the current vs. time record (1 Amp = 96,500 mol $e^-$/s) and corresponds to a transfer of 2.23 moles of electrons. With geochemical data from only one side of the active anode, we begin by assuming that similar reactions occurred on both faces of the anode disc, or that the measured sediment profiles reflect reactions associated with half of the current (1.115 moles of electrons).

Significant concentration gradients in iron and sulfur species started 3 cm above the active anode (Figures 2 and 3). Thus, this distance times the surface area of one face of the anode plus one half the volume of holes in the anode seem to define a critical sediment reaction layer for the active fuel cell

*Table 2.* Estimated contributions of solid phase reactants to the fuel cell anodic mechanism.

| Units of change | Primary reactants oxidized[a] | | Products produced | | |
|---|---|---|---|---|---|
| | FeS | $FeS_2$ | $S^o$ | $SO_4^{2-}$ | $Fe^{2+}$ |
| mmoles | $-72 \pm 14$ | $-74 \pm 37$ | $83 \pm 105$ | $137 \pm 17$ | $146 \pm 51$ |

These calculations are based on a simple electron balance for one side of the anode and assume that only FeS and $FeS_2$ are major fuels. Reactions (1) and (2) are considered to be the primary anodic oxidation reactions of these fuels, followed by further oxidation of $S^0$. The reactive sediment layer is assumed to have a volume = 5661 $cm^3$ and 1115 mmoles of electrons are estimated to have been harvested from the reactive layer.

[a] $n = V_{SP}*\rho*(C_{max}-C_{min})/2$; with $n$ = number of moles of a sulfur mineral consumed, $V_{SP}$ = volume of solid phase in the sediment layer = $(1-P)*V$ = 1698 $cm^3$, $P$ = porosity = 70%, $\rho$ = solid phase density = 2.5 $g/cm^3$, $C_{max}$ = maximal concentration at outer boundary of reactive layer, $C_{min}$ = minimum concentration at anode surface.

experiment with a volume of 5661 $cm^3$. It is possible to estimate the amount of solid-phase sulfur oxidized within this volume by integrating over the approximately linear concentration gradients of AVS and CRS. By this approach and the assumption that the losses of AVS and CRS represent losses of FeS and pyrite respectively, the solid-phase profiles from Yaquina Bay predict oxidation of $72 \pm 14$ mmoles FeS and $74 \pm 37$ mmoles pyrite (Table 2). By reactions (1) and (2) these estimates suggest the production of on the order of 292 mmoles of electrons and 220 mmoles of elemental sulfur. To balance the electrons transferred to the anode, 62% of the elemental sulfur produced by the oxidation of the sulfide minerals may be assumed to have been further oxidized to sulfate. (The reaction mechanism leading to this oxidation is not critical to this calculation.) The remaining 38% of $S^0$ (83 mmoles) could have become available for microbial activity (uncoupled to the anode) or could have accumulated. This amount of elemental sulfur if separated from the anode would correspond to an average enrichment of 20 $\mu$mol $S^0$/g dry sediment in the 3 cm thick sediment layer above the anode. Certainly there are large uncertainties in these estimates (Table 2), but they help illustrate that the oxidation of metal sulfides is a feasible anodic mechanism. Consistent with this, the accumulation of sulfur at the electrode surface was detected by electron microprobe analysis. Moreover, element profiles across the biofilm indicate a dilution effect as a function of the distance from the anode, with a sulfur concentration in the biofilm about four times lower than at the electrode surface (Figure 5). We have not attempted to account for all the dissolved $Fe^{2+}$ or sulfate produced by this balance because these species would have diffused from the sediment reaction volume continuously over the seven-month experiment.

*Consequences of sulfur deposition*

It is possible to estimate the maximum thickness of a $S^0$-film that would deposit uniformly at an electrode surface based on the number of electrons transferred

during an experiment. Using the density of elemental sulfur ($\rho_{S^0}$ = 2.07 g/cm$^3$), the maximum thickness of a film of pure $S^0$ would be

$$t = (n_{S^0} M_{S^0})/(A\rho_{S^0}) \quad (5)$$

where $A$ corresponds to the electrode surface area, $M_{S^0}$ is the molecular mass of sulfur (32 g/mol), and $n_{S^0}$ is the number of moles of sulfur deposited. If $n_{S^0}$ = 83 mmoles as suggested by Table 2, then the thickness of the $S^0$-film on the anode recovered from Yaquina Bay should have been no more than 2.4 $\mu$m. Microprobe analyses (Figure 5) showed a sulfur enrichment corresponding to a layer of about 20 $\mu$m but with a sulfur concentration of only 2 wt% at the most in this layer. Because sulfide sources may have varied over time and the Yaquina Bay anode had periods of inactivity, the missing $S^0$ may reflect periods of biofilm growth and utilization of sulfur when the anode was not drawing current. The deposition of other elements, including Si, Fe and P, explains a thicker layer of sulfur-enriched material (i.e., not pure $S^0$) compared to the theoretical estimation.

The current produced by the relatively short-term laboratory fuel cell also resulted from sulfide oxidation. The current integration over time and the conversion to moles of electrons was used to estimate that 64.7 $\mu$mol of $S^0$ may have been produced. By similar reasoning to that applied for the Yaquina Bay experiment, a 0.49 $\mu$m-thick film of sulfur should have deposited on the laboratory electrode. This is thinner than the microprobe beam size used for the surface analyses making it difficult to detect. However, Figure 6b indicates that S was irregularly distributed on the active electrode. This is in agreement with McGuire et al. (2001) who have reported that elemental sulfur as product of the oxidation of reduced sulfur does not form a continuous film, but deposits as discrete patches, dispersed randomly across the sample surface.

### *Biogeochemical cycle of sulfur*

By reconciling the measured geochemical effects of the fuel cell deployed in Yaquina Bay with the microbial analyses of Holmes et al. (2004b) it seems likely that a unique biogeochemical cycle (Figure 7) was created or amplified by the fuel cell. This cycle appears also to have been critical for sustaining energy over 7 months. The cycle was initiated by the nearly ubiquitous degradation of organic matter (Figure 3a) by sulfate-reducing bacteria in the anoxic sediment of the Yaquina Bay estuary. This anaerobic metabolism generated dissolved sulfide (Figure 2a), but most of this sulfide reacted with Fe oxides or dissolved $Fe^{2+}$ to produce FeS and $FeS_2$ which accumulated with sediment depth (Figure 3e and f). In the presence of the active fuel cell, any available dissolved sulfide was electroactive at the anode surface as confirmed by the two-chamber experiments (Figure 6a). Once dissolved sulfide became limiting, reduced sulfur minerals provided electrons to the seafloor fuel cell (Figure 3e and f). Although the oxidation of pyrite under anaerobic conditions

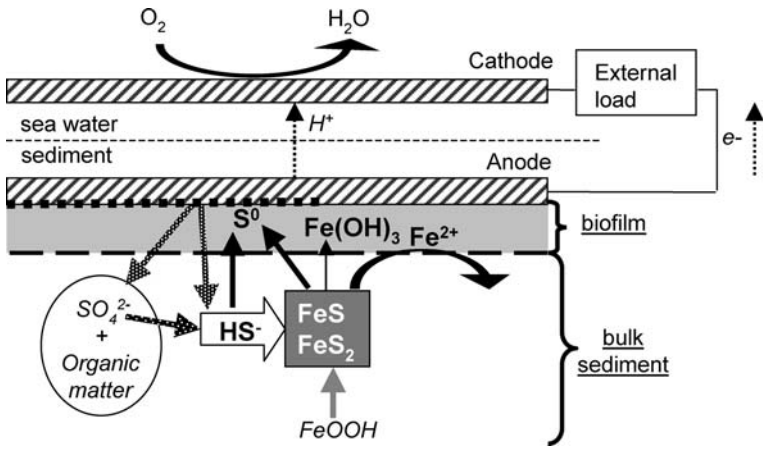


*Figure 7.* Biogeochemical cycle amplified by the fuel cell mechanism. ➡ Electrochemical reaction; ⇒ sulfate-reducing bacteria; ⇒ $S^0$-disproportionation; ⇒ geochemical reactions. The degree to which iron is oxidized electrochemically at the anode is uncertain, as discussed in the text.

may be controversial as a process in nature, it can be driven electrochemically (Hamilton and Woods 1981). Elemental sulfur is suggested to be the main end product of these electrochemical reactions with dissolved and solid-phase sulfides, because sulfur accumulated at the active anode surface (Figure 5) and also because of the dominant abundance of *Desulfobulbus*/*Desulfocapsa* spp. (Table 1) (Holmes et al. 2004b). To balance the current production, part of the $S^0$ appears to have been further oxidized to sulfate, supplying more electrons to produce current. This reaction may have been abiotic (Turcotte et al. 1993; Zhu et al. 1994) and/or microbially mediated (Holmes et al. 2004a) passing electrons directly from $S^0$ to graphite. Alternatively, $S^0$ disproportionation by *Desulfobulbus*/*Desulfocapsa* spp. (Lovley and Phillips 1994; Finster et al. 1998) may have regenerated both sulfate and sulfide. Reoxidation of this sulfide at the anode surface would result in the same electron balance. As a consequence of the dissolution of sulfide minerals, $Fe^{2+}$ was released and accumulated near the anode surface (Figure 2c). Some iron may have precipitated as Fe oxides, coating the graphite surface with a thin layer (Figure 5). For the long-term utility of seafloor fuel cell devices, these reaction products may be of greatest concern, either because they may block parts of the anode surface leading to passivation (Allen and Hickling 1957), or because they enhance current production by providing a novel microbial habitat.

## Summary and conclusions

Biogeochemical and electrochemical processes occurring at the anode of a prototype seafloor fuel cell were studied by analyzing changes in sediment composition and deposits on the anode surface. This approach helped to

identify the most probable reactions influencing the buried electrode and to relate these reactions to the fuel cell mechanism.

The fuel cell exhibited a potential difference of ~0.75 V at open circuit in a coastal environment. The anode potential was regulated by the microbial activity that reduces sulfate to sulfide in the absence of oxygen. Sterile laboratory fuel cells with $HS^-$ as sole electron donor confirmed an abiotic mechanism may produce current densities comparable to fuel cells in the field. However, the Yaquina Bay experiment showed that solid-phase AVS and CRS (probably representing FeS and $FeS_2$) become the dominant chemical electron donors to the fuel cell when concentrations of dissolved sulfide are low. The fact that the active fuel cell anode selected for bacteria able to disproportionate $S^0$ (Holmes et al. 2004b) indicated other possible electron transfer mechanisms and a localized biogeochemical cycle.

What is not yet known is how unique are the interactions revealed by this study. Given that most nearshore marine sediments contain abundant sulfide minerals and organic matter, and that dissimilatory metal or sulfur reducing bacteria are common, it is likely these effects can be easily recreated and relied on for energy harvesting. Future experiments will concentrate on reversing surface reactions that may deactivate electrodes.

## Acknowledgements

This research was supported by Grant N00014-02-1-0480 from the Office of Naval Research. Additional salary support was provided by the National Science Foundation Grant OCE-0242048. Special thanks go to Andy Ross, Chi Meredith, Daniel Lowry, and Margaret Sparrow for analytical assistance. Roger Nielsen, Ed Kohut and Mike Rowe helped with the surface microprobe analyses. In addition, we thank Maggie Sommer, Robert Emmett, Todd Bridgeman, Tonya Builder, William Hanshumacher, David Jacobson, and Mara Spencer for diving assistance. Leonard Tender helped design and equip the field experiment. Two anonymous reviewers provided helpful feedback on interpretations.

## References

Allen P.L. and Hickling A. 1957. Electrochemistry of sulfur. Part 1. Overpotential in the discharge of the sulfide ion. Trans. Faraday Soc. 53: 1626–1635.

Allen R.E. and Parkes R.J. 1995. Digestion procedures for determining reduced sulfur species in bacterial cultures and in ancient and recent sediments. In: Vairavamurthy M.A. and Schoonen M.A.A. (ed.), Geochemical Transformations of Sedimentary Sulfur. American Chemical Society, Washington D.C., pp. 243–257.

Ateya B.G. and Alkharafi F.M. 2002a. Anodic oxidation of sulfide ions from chloride brines. Electrochem. Commun. 4: 231–238.

Ateya B.G. and Alkharafi F.M. 2002b. Electrochemical removal of hydrogen sulfide from geothermal brines. Electrochem. Soc. Proc. 15: 87–98.

Ateya B.G., Alkharafi F.M. and Al-Azab S.S. 2003. Electrodeposition of sulfur from sulfide contaminated brines. Electrochem. Solid-State Lett. 6: C137–C140.

Baas Becking L.G.M., Kaplan I.R. and Moore D. 1960. Limits of the natural environment in terms of pH and oxidation-reduction potentials. J. Geol. 68: 243–284.

Bacon F.T. and Fry T.M. 1970. Review lecture: the development and practical application of fuel cells. Proceedings of the Royal Society of London. Series A, Math. Phys. Sci. 334: 427–452.

Berner R.A. 1963. Electrode studies of hydrogen sulfide in marine sediments. Geochim. Cosmochim. Acta 27: 563–575.

Berner R.A. 1964. Stability fields of iron minerals in anaerobic marine sediments. J. Geol. 72: 826–834.

Berner R.A. 1970. Sedimentary pyrite formation. Am. J. Sci. 268: 1–23.

Berner R.A. 1978. Sulfate reduction and the rate of deposition of marine sediments. Earth Planet. Sci. Lett. 37: 492–498.

Berner R.A. 1984. Sedimentary pyrite formation: an update. Geochim. Cosmochim. Acta 48: 605–615.

Berner R.A. 1985. Sulfate reduction, organic matter decomposition and pyrite formation. Philosophical Transactions of the Royal Society of London. Series A, Math. Phys. Sci. 315: 25–37.

Berner R.A. and Raiswell R. 1984. C/S method for distinguishing freshwater from marine sedimentary rocks. Geology 12: 365–368.

Bond D.R., Holmes D.E., Tender L.M. and Lovley D.R. 2002. Electrode-reducing microorganisms that harvest energy from marine sediments. Science 295: 483–485.

Bond D.R. and Lovley D.R. 2003. Electricity production by *Geobacter sulfurreducens* attached to electrodes. Appl. Environ. Microbiol. 69: 1548–1555.

Canfield D.E. 1989a. Reactive iron in marine sediments. Geochim. Cosmochim. Acta 53: 619–632.

Canfield D.E. 1989b. Sulfate reduction and oxic respiration in marine sediments: implications for organic carbon preservation in euxinic environments. Deep-Sea Res. 36: 121–138.

Canfield D.E., Raiswell R., Westrich J.T., Reaves C.M. and Berner R.A. 1986. The use of chromium reduction in the analysis of reduced inorganic sulfur in sediments and shales. Chem. Geol. 54: 149–155.

Cline J.D. 1969. Spectrophotometric determination of hydrogen sulfide in natural waters. Limnol. Oceanogr. 14: 454–458.

Ferdelman T.G., Church T.M. and Luther G.W.III 1991. Sulfur enrichment of humic substances in Delaware salt marsh sediment core. Geochim. Cosmochim. Acta 55: 979–988.

Finster K., Liesack W. and Thamdrup B. 1998. Elemental sulfur and thiosulfate disproportionation by *Desulfocapsa sulfoexigens* sp. nov., a new anaerobic bacterium isolated from marine surface sediment. Appl. Environ. Microbiol. 64: 119–125.

Fossing H. and Jørgensen B.B. 1989. Measurement of bacterial sulfate reduction in sediments: evaluation of a single-step chromium reduction method. Biogeochemistry 8(6): 205–222.

Goldhaber M.B. and Kaplan I.R. 1975. Controls and consequences of sulfate reduction rates in recent marine sediments. Soil Sci. 119: 42–55.

Greaves C. 1970. The direct conversion of chemical energy to electricity. Phys. Edu. 5: 18–24.

Hamilton I.C. and Woods R. 1981. An investigation of surface oxidation of pyrite and pyrrhotite by linear potential sweep voltammetry. J. Electroanal. Chem. 118: 327–343.

Holmes D.E., Bond D.R. and Lovley D.R. 2004a. Electron transfer by *Desulfobulbus propionicus* to Fe(III) and graphite electrodes. Appl. Environ. Microbiol. 70: 1234–1237.

Holmes D.E., Bond D.R., O'Neil R.A., Reimers C.E., Tender L.M. and Lovley D.R. 2004b. Microbial communities associated with electrodes harvesting electricity from a variety of aquatic sediments. Microb. Ecol 48: 178–190.

Holmes P.R. and Crundwell F.K. 2000. The kinetics of the oxidation of pyrite by ferric ions and dissolved oxygen: an electrochemical study. Geochim. Cosmochim. Acta 64: 263–274.

Jones D.A. 1996. Principles and Prevention of Corrosion. Prentice Hall, Englewood Cliffs, New Jersey.

Jørgensen B.B. 1977. The sulfur cycle of a coastal marine sediment (Limfjorden, Denmark). Limnol. Oceanogr. 22: 814–832.

Jørgensen B.B. 1982. Ecology of the bacteria of the sulfur cycle with special reference to anoxic-oxic interface environments. Phil. Trans. Royal Soc. London, Series B 298: 543–561.

Jørgensen B.B. and Fenchel T. 1974. The sulfur cycle of a marine sediment model system. Mar. Biol. 24: 189–201.

Keil R.G., Tsamakis E., Fuh C.B., Giddings J.C. and Hedges J.I. 1994. Mineralogical and textural controls on the organic composition of coastal marine sediments: hydrodynamic separation using SPLITT-fractionation. Geochim. Cosmochim. Acta 58: 879–893.

Kostka J.E. and Luther G.W. III. 1994. Partitioning and speciation of solid iron in saltmarsh sediments. Geochim. Cosmochim. Acta 48: 1701–1710.

Lin S., Huang K.-M. and Chen S.-K. 2002. Sulfate reduction and iron sulfide mineral formation in the southern East China continental slope sediment. Deep-Sea Res. 49: 1837–1852.

Lin S. and Morse J.W. 1991. Sulfate reduction and iron sulfide mineral formation in the Southern East China continental slope sediment. Am. J. Sci. 29: 55–89.

Lovley D.R. and Phillips E.J.P. 1994. Novel processes for anaerobic sulfate production from elemental sulfur by sulfate reducing bacteria. Appl. Environ. Microbiol. 60: 2394–2399.

McDougall A. 1976. Fuel Cells. Wiley & Sons, New York.

McGuire M.M., Jallad K.N., Ben-Amotz D. and Hamers R.J. 2001. Chemical mapping of elemental sulfur on pyrite and arsenopyrite surfaces using near-infrared Raman imaging microscopy. Appl. Surf. Sci. 178: 105–115.

Measures C.I., Yuan J. and Resing J.A. 1995. Determination of iron in seawater by flow injection-analysis using in-line preconcentration and spectrophotometric detection. Mar. Chem. 50: 3–12.

Moses C.O. and Herman J.S. 1990. Pyrite oxidation at circumneutral pH. Geochim. Cosmochim. Acta 55: 471–482.

Moses C.O., Nordstrom D.K., Herman J.S. and Mills A.L. 1987. Aqueous pyrite oxidation by dissolved oxygen and by ferric iron. Geochim. Cosmochim. Acta 51: 1561–1571.

Müller P.J. and Suess E. 1979. Productivity, sedimentation rate, and sedimentary organic matter in the oceans - I. Organic carbon preservation. Deep-Sea Res. 26: 347–1362.

Mycroft J.R., Bancroft G.M., McIntyre N.S., Lorimer J.W. and Hill I.R. 1990. Detection of sulphur and polysulphides on electrochemically oxidized pyrite surfaces by X-ray photoelectron spectroscopy and Raman spectroscopy. J. Electroanal. Chem. 292: 139–152.

Pokrovski G.S., Schott J., Farges F. and Hazemann J.-L. 2003. Iron (III)–silica interactions in aqueous solution: insights from X-ray absorption fine structure spectroscopy. Geochim. Cosmochim. Acta 67: 3559–3573.

Powell H.S. 1980. Decomposition of Organic Matter in Estuarine Sediments by Sulfate Reduction: A Field Study from Yaquina Bay and Sediment Incubation Experiments. M.S. thesis, Oregon State University, Corvallis.

Ransom B., Kim D., Kastner M. and Wainwright S. 1998. Organic matter preservation on continental slopes: importance of mineralogy and surface area. Geochim. Cosmochim. Acta 62: 1329–1345.

Reimers C.E., Tender L.M., Fertig S.J. and Wang S. 2001. Harvesting energy from the marine sediment–water interface. Environ. Sci. Technol. 35: 192–195.

Resing J.A. and Mottl M.J. 1992. Determination of manganese in seawater using flow injection analysis with on-line preconcentration and spectrophotometric detection. Anal. Chem. 64: 2682–2687.

Rimstidt J.D. and Vaughan D.J. 2003. Pyrite oxidation: a state-of-the-art assessment of the reaction mechanism. Geochim. Cosmochim. Acta 67: 873–880.

Rozan T.F., Taillefert M., Trouwborst R.E., Glazer B.T. and Ma S. 2002. Iron-sulfur-phosphorous cycling in the sediments of a shallow coastal Bay: implications for sediment nutrient release and benthic macroalgal blooms. Limnol. Oceanogr. 47: 1346–1354.

Ryckelynck N. 2004. Understanding the Anodic Mechanism of a Seafloor Fuel Cell. M.S. thesis, Oregon State University, Corvallis.

Schippers A. and Jørgensen B.B. 2002. Biogeochemistry of pyrite and iron sulfide oxidation in marine sediments. Geochim. Cosmochim. Acta 66: 85–92.

Stookey L.L. 1970. Ferrozine – a new spectrophotometric reagent for iron. Anal. Chem. 42: 779–781.

Stumm W. 1992. Chemistry of the Solid-Water Interface Processes at the Mineral-Water and Particle Water Interface in Natural Systems. Wiley, New York.

Tender L.M., Reimers C.E., Stecher H.W.III, Holmes D.E., Bond D.R., Lowy D.A., Pilobello K., Fertig S.J. and Lovley D.R. 2002. Harnessing microbially generated power on the seafloor. Nat. Biotechnol. 20: 821–825.

Thamdrup B. and Canfield D.E. 1996. Pathways of carbon oxidation in continental margin sediments off central Chile. Limnol. Oceanogr. 41: 1629–1650.

Thamdrup B., Fossing H. and Jørgensen B.B. 1994. Manganese, iron and sulfur cycling in a coastal marine sediment, Aarhus Bay, Denmark. Geochim. Cosmochim. Acta 58: 5115–5129.

Turcotte S.B., Benner R.E., Riley A.M., Li J., Wadsworth M.E. and Bodily D.M. 1993. Surface analysis of electrochemically oxidized metal sulfides using Raman spectroscopy. J. Electroanal. Chem. 347: 195–205.

Verardo D.J., Froelich P.N. and Andrew M. 1990. Determination of organic carbon and nitrogen in marine sediments using the Carlo Erba NA-1500 analyzer. Deep-Sea Res. 37: 157–165.

Vijh A.K. 1970. Electrochemical principles involved in a fuel cell. J. Chem. Edu. 47: 680–682.

Walsh J.J., Premuzic E.T., Gaffney J.S., Rowe G.T., Hartbottle G., Stoenner R.W., Balsam W.L., Betzer P.R. and Macko S.A. 1985. Organic storage of $CO_2$ on the continental slope off the mid-Atlantic bight, the southeastern Bering Sea, and the Peru coast. Deep-Sea Res. 32: 853–883.

Wang Q. and Morse J.W. 1996. Pyrite formation under conditions approximating those in anoxic sediments. I. Pathway and morphology. Mar. Chem. 52: 99–121.

Wijsman J.W.M., Middelburg J.J., Herman P.M.J., Böttcher M.E. and Heip C.H.R. 2001. Sulfur and iron speciation in surface sediments along the northwestern margin of the Black Sea. Mar. Chem. 74: 261–278.

Zhabina N.N. and Volkov I.I. 1978. A method of determination of various sulfur compounds in sea sediments and rocks. In: Krumbein W.E. (ed.), Environmental Biogeochemistry; Methods, metals and assessment, Vol. 3. Ann Arbor Science Publishers, Mich, pp. 735–745.

Zhu X., Li J. and Wadsworth M.E. 1994. Characterization of surface layers formed during pyrite oxidation. Colloid Surf. A: Physicochem. Eng. Asp. 93: 201–210.